Received: 27 February 2024 | Revised: 5 May 2024 | Accepted: 5 May 2024

DOI: 10.1002/app.55710

RESEARCH ARTICLE

Journal of Applied Polymer Science WILEY

Mechanical and thermal characterization of elastomer modified polypropylene hybrid composites reinforced with hazelnut shell and wollastonite fillers

İdris Karagöz[1] | Kenan Büyükkaya[2] | Halil Demirer[3] | Mehmet Mudu[1] | İlyas Kartal[3]

[1]Department of Polymer Materials Engineering, Yalova University, Yalova, Turkey

[2]Technical Sciences Vocational High School, Giresun University, Giresun, Turkey

[3]Department of Metallurgy and Materials Engineering, Marmara University, Istanbul, Turkey

Correspondence
İdris Karagöz, Department of Polymer Materials Engineering, Yalova University, 77200 Yalova, Turkey.
Email: idris.karagoz@yalova.edu.tr

Abstract

The demand for sustainable and recyclable materials in industrial applications has led to a surge in interest in green composites, particularly those incorporating natural fillers derived from agro-food industry waste. This study investigates the mechanical and thermal properties of polypropylene (PP) hybrid composites filled with hazelnut shell and wollastonite, along with the effect of styrene-ethylene/butylene-styrene (SEBS) and SEBS-g-maleic anhydride (SEBS-g-MA) compatibilizers. Various characterization techniques, including tensile, flexural, and impact tests, as well as differential scanning calorimetry (DSC), thermogravimetry (TGA), and scanning electron microscopy (SEM) analyses, were employed to evaluate the composites. Results demonstrate that the addition of wollastonite significantly improves mechanical properties, while hazelnut shell filler affects thermal behavior and stability. SEBS and SEBS-g-MA compatibilizers enhance impact resistance; however, they lead to a decrease in other mechanical properties. DSC and TGA analyses demonstrate changes in crystallization behavior and thermal stability due to filler and compatibilizer incorporation. SEM microstructure images show the distribution of SEBS and SEBS-g-MA within the composite structure, affecting mechanical and thermal properties. Overall, this study highlights the importance of filler selection, compatibilizer addition, and their distribution in attaining desired properties for industrial applications. Future research should focus on optimizing formulations for specific uses and assessing long-term performance under real-world conditions.

KEYWORDS

green composite, hazelnut shell, hybrid composite, SEBS, SEBS-g-MA, wollastonite

1 | INTRODUCTION

The contemporary industry is increasingly prioritizing the creation of sustainable and recyclable goods, motivated by the swift depletion of natural resources and escalating environmental apprehensions. In recent years, there has been a growing interest in using natural resources obtained from agro-food industry wastes or by-products in polymer-based composites due to their low environmental impact, recyclability, and ease of processing.[1] These composites are commonly referred to as "green composites."[2,3]

Products made from green composites find extensive use in industries such as automotive, furniture, construction, and packaging.[2–5] Various natural fillers, including cellulose,[4,6] wood flour,[7] oak sawdust,[8] bagasse fiber,[9] eggplant (Solanum melongena) stalks,[10] hazelnut shell,[8,11–16] walnut shell, sunflower husk,[16] almond shell,[17] cocoa,[18] and eucalyptus fiber (Eucalyptus grandis),[19] are employed in the production of green composites. Additionally, materials such as coal,[20] basalt,[21] calcium carbonate, perlite, and potassium dichromate,[13] glass fiber,[14] mica, kaolin, wollastonite, silica, and so on,[22] are added to enhance the mechanical and thermal properties of green composites, resulting in hybrid composites.

The production of hybrid composites faces several significant challenges, including the difficulty of adjusting the necessary composition for desired mechanical properties, high costs,[5,23] poor machinability, dimensional instability, and low ductility.[22,24] Liu et al.[24] observed significant variations in mechanical properties based on particle/fiber size, while Thakur et al.[23] emphasized the influence of formulation on machinability. Nuñez et al.[7] noted that the addition of maleic anhydride (MA) improved the dispersion of wood flour in the polypropylene (PP) matrix. Barczewski et al.[16] reported that particle-shaped fillers increased hardness and stiffness, fiber-shaped additions increased mechanical properties, and hazelnut shell emerged as the most suitable filler for green composites. In the realm of thermoplastic materials, they are preferred over thermosets in hybrid composite production due to their ability to be reshaped with heat, recycled, and their positive environmental impact.[2,4] Among thermoplastic materials, PP is more commonly used than other polymer types.[25–27]

Researchers have emphasized the need for in-depth studies in academia and industry on crucial aspects such as new formulations, processing methods, and composite material design.[4,5,22] In the near future, the outcomes of these new studies are anticipated to lead to large-scale production cost reductions and improvements in mechanical properties, particularly in the automotive sector for hybrid composites, covering body panels, outdoor panels, and structural parts. The application of these composites is also expected to extend to various sectors such as aviation, construction, and agriculture, where a combination of metals and polymers is essential.[5,22–24] Upon reviewing the aforementioned studies, it becomes evident that the development of new formulations is vital to facilitate the widespread industrial use of green composites, ultimately enabling cost-effective production.

This study aims to investigate the impact of formulations using hazelnut shell, wollastonite, SEBS, and SEBS-g-MA at various ratios and contents on the thermal, mechanical, and microstructural properties of PP matrix hybrid composites. Mechanical properties were assessed through tensile, bending, and Izod impact tests. The compatibility of PP composites, with SEBS and SEBS-g-MA, was studied using differential scanning calorimetry (DSC), thermogravimetry (TGA), and Fourier-transform infrared spectroscopy (FTIR). To verify miscibility, the morphology of the blends was examined through scanning electron microscopy (SEM). The results indicate that SEBS-g-MA serves as an effective compatibilizer in PP systems through promoting interfacial interactions.

2 | MATERIALS AND METHODS

2.1 | Materials

Petoplen PP-MH418 (PETKİM, Turkey), which is an isotactic PP, was utilized as the matrix. Ciba Irgafos® 168 FF by BASF, tris(2,4-di-tert.-butylphenyl) phosphite (Ciba Specialty Chemicals, Sweden), was employed for stabilization. VISCOWAX® 262 OXIDISED PE-WAX (ERAL, Turkey) was used to facilitate processing. Hazelnut shell flour (HNSF-particle size ≤150 μm) and acicular wollastonite (W; Nyglos® 8) with a large aspect ratio of ∼19/1 (∼150/8 μm) supplied by Nyco Minerals Ltd. were used as fillers. The composition of hazelnut shell consists of 54.61% holocellulose (29.94% cellulose and 24.67% hemicellulose) and 31.87% lignin.[28] The prominent compounds in the chemical composition of wollastonite are Al_2O_3 at 0.40%, CaO at 46.36%, Fe_2O_3 at 0.77%, and SiO_2 at 51.6%, respectively.[29] SEBS (Kraton G 1652, Shell Chemicals), and SEBS-g-MA (Kraton FG 190IX, Shell Chemicals), were employed as elastomeric compatibilizers. The formulations and sample codes used in the study are given in Table 1.

2.2 | The sample preparation through extrusion and injection molding process

The formulations provided in Table 1 were processed into granules using a Gülnar-brand twin-screw extruder

(Turkey) with a screw length-to-diameter ratio (L/D) of 24 and a screw diameter (Ø) of 16 mm. The materials were thoroughly mixed at funnel-nozzle temperatures of 30/110/170/190°C and a rotation speed of 250 rpm. The extrusion process, screw rotation direction (clockwise), and regions of resistance temperatures are illustrated in detailed Figure 1. Following the granulation process, the samples were dried at 60°C for 3 h, and subsequently placed in a desiccator to ensure they remained dry and did not absorb moisture until the injection process. Tensile (ISO 527) and impact (ISO 180) test samples were molded using an Engel-brand Spex Victory 80 model injection molding machine (Germany) with a closing force of 800 kN. The injection molding procedure adhered to the specifications outlined in Table 2, in accordance with ISO 294 standards.

2.3 | Characterization

Tensile tests were conducted in accordance with ISO 527-1 standards, and 3-point flexural tests were performed following ISO 178 standards using the Zwick Z010 model machine with a 10 kN load cell. Izod impact tests, with three different notch radii ($R = 0.25/1/2$ mm), were carried out on an Instron Ceast 9050 model machine with a 5.4 Joule hammer, in compliance with ISO 180 standards. Tensile tests were conducted at room temperature and at a drawing rate of 50 mm/min on 5 Type 1A specimens, as defined in ISO 527-1 standard, with a thickness limited to 4 mm, and averages were calculated. Three-point flexural tests were performed at room temperature and at a bending rate of 5 mm/min on 5 bar-shaped specimens defined in ISO 178 standard, with a thickness of 4 mm, a width of 10 ± 0.2 mm, and a length ≥80 mm, and averages were calculated. For impact tests, 10 bar-shaped specimens measuring 4 × 10 × 80 mm were used for each notch parameter, and averages were taken. Hardness measurements, based on the Shore *D* scale, were conducted using a Zwick Roel model machine, adhering to ISO 48-4 standards.

The DSC test was conducted using a Seiko DSC 7020 model equipment following ASTM D3418-21 standards. Heat deflection temperature (HDT) tests were performed on an Instron Ceast HV3 model equipment in accordance with ASTM D1525-17 standards. Thermogravimetric analysis (TGA) tests were carried out on a Seiko TG/DTA6300 model equipment following ISO 11358-1 standards. FTIR tests were conducted using a Perkin Elmer Spectrum 100 FT-IR model equipment following ASTM D6348-12 standards. The DSC melt peak analyses were used to calculate the crystallinity percentages (X_c) using the equation provided in Equation (1), and the crystal lamellae thicknesses (λ) were determined using the Gibbs–Thomson equation given in Equation (2).[30] In calculations, the enthalpy of 100% crystalline state (ΔH_m°)

TABLE 1 Sample formulations and codes.

Sample code	PP (%)	W (%)	HNSF (%)	SEBS (%)	SEBS-g-MA (%)
PP01	100	-	-	-	-
PP02	80	20	-	-	-
PP03	80	15	5	-	-
PP04	80	10	10	-	-
PP05	80	5	15	-	-
PP06	77	10	10	3	-
PP07	74	10	10	6	-
PP08	71	10	10	9	-
PP09	77	10	10	-	3
PP10	74	10	10	-	6
PP11	71	10	10	-	9

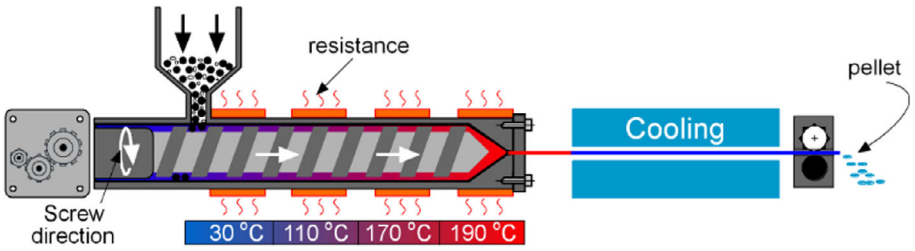

FIGURE 1 The extrusion process and depiction of temperature zones. [Color figure can be viewed at wileyonlinelibrary.com]

TABLE 2 Injection process parameters for the specimen preparation.

Parameters	Value	Temperatures	Value
Injection rate	50 mm/s	Nozzle	200°C
Injection pressure	100 bar	Metering zone	190°C
Holding pressure	40 kN	Transition zone	175°C
Holding time	3 s	Feed zone	165°C
Cooling time	10 s	Mold surface	40 ± 5°C

for PP was considered as 209 J/g, the equilibrium melting temperature (T_m°) was set at 174°C, and the surface energy of the crystals (δ_e) was assumed to be 29 mJ/m^2, and Φ in the formula represents the weight fraction of residues in the matrix.

$$X_c = \frac{\Delta H_m}{\Delta H_m^\circ (1-\Phi)} \times 100 \quad (1)$$

$$\frac{T_m}{T_m^\circ} = 1 - \frac{2\delta_e}{\Delta H_m} \quad (2)$$

The fractured surfaces of impact-tested samples were examined under an Inspect S50 model SEM to visualize microstructures. To analyze the morphology of the elastomeric phase (SEBS and SEBS-g-MA) in the composites via SEM, a specific etching procedure was conducted. The chosen samples underwent rapid cooling in liquid nitrogen followed by fracturing. Following this, the surfaces were etched using THF at 60°C for a duration of 30 min, and then dried under vacuum at room temperature for 24 h. Subsequently, SEM micrographs were captured from the fractured surfaces of the samples.

3 | RESULTS AND DISCUSSION

3.1 | FT-IR test results

Figure 2 displays the FT-IR spectra for PP and its composites. For PP, the FT-IR peaks include the symmetric stretching of the nonsymmetrical CH3 group's C—H bond at 2950 cm^{-1}, the symmetric stretching of the nonsymmetrical CH2 group's C—H bond at 2920 cm^{-1}, the symmetric stretching of the CH3 group's C—H bond at 2870 cm^{-1}, the bending of the CH3 group's C—H bond at 1456 cm^{-1}, the bending of the CH3 group's C—H bond at 1376 cm^{-1}, the stretching of the C—H bond at 1166 cm^{-1}, the chain stretching vibration of C—C at 996 cm^{-1}, the bond vibration of C—C at 973 cm^{-1}, the bending of the C—H bond at 840 cm^{-1}, and the stretching of the C—C bond at 808 cm^{-1}, all observed in all samples. All spectra closely resemble PP's known characteristic peaks.[29,31] No IR splitting resulting from intermolecular or crystalline packing was observed, as the chains are too far apart. In fact, the intermolecular forces are too small for crystal field splitting to be observed.[32]

Only in samples PP09 and PP10, peaks at 3671 and 3800 cm^{-1} correspond to hydroxyl groups. These peaks may be related to the presence of potential polar groups derived from additives.[29] This situation could also be associated with changes in band intensity among mixtures with different concentrations of the same additive. For samples coded as PP09 and PP10, the characteristic peaks of the SEBS addition are observed between 2990 and 2880 cm^{-1}. The absence of these peaks in sample PP11 indicates the grafting of SEBS chains, forming a covalent bond between SEBS and SEBS-g-MA and the polymer.[33] When comparing the FTIR results of all samples, there is no noticeable chemical interaction. However, MA caused peaks to shift. Similarly, depending on the formulation ratios of the mixture, changes are observed in all peak heights.

3.2 | Mechanical test results

The results of tensile and flexural tests are presented in Table 3. The stress–strain curves for all composites' tensile tests are provided in Figure 3. With the exception of impact strength, the composite coded as PP02 with a 20% wollastonite filler exhibited superior mechanical properties compared with pure PP. In composites where hazelnut shell and wollastonite were added as filler materials in equal proportions (both 10%), a decrease in the proportion of wollastonite led to a decline in all mechanical properties of the composite. Wollastonite demonstrated a more pronounced effect on mechanical properties compared with hazelnut shell filler, and this improvement is believed to be attributed to the long and thin fibrous structure of wollastonite.[34] Previous studies have consistently noted that an increase in the proportion of organic filler in the structure correlates with a decrease in mechanical properties.[35–37] Upon the addition of SEBS and SEBS-g-MA to the mixture with an equal ratio of hazelnut shell and wollastonite, it resulted in a reduction in tensile strength, tensile modulus, flexural strength, and flexural modulus, while concurrently enhancing impact strength.

The results of hardness and impact tests are provided in Table 4. This increase in impact strength became more pronounced with the higher ratio of SEBS and SEBS-g-MA in the structure. It is believed that this

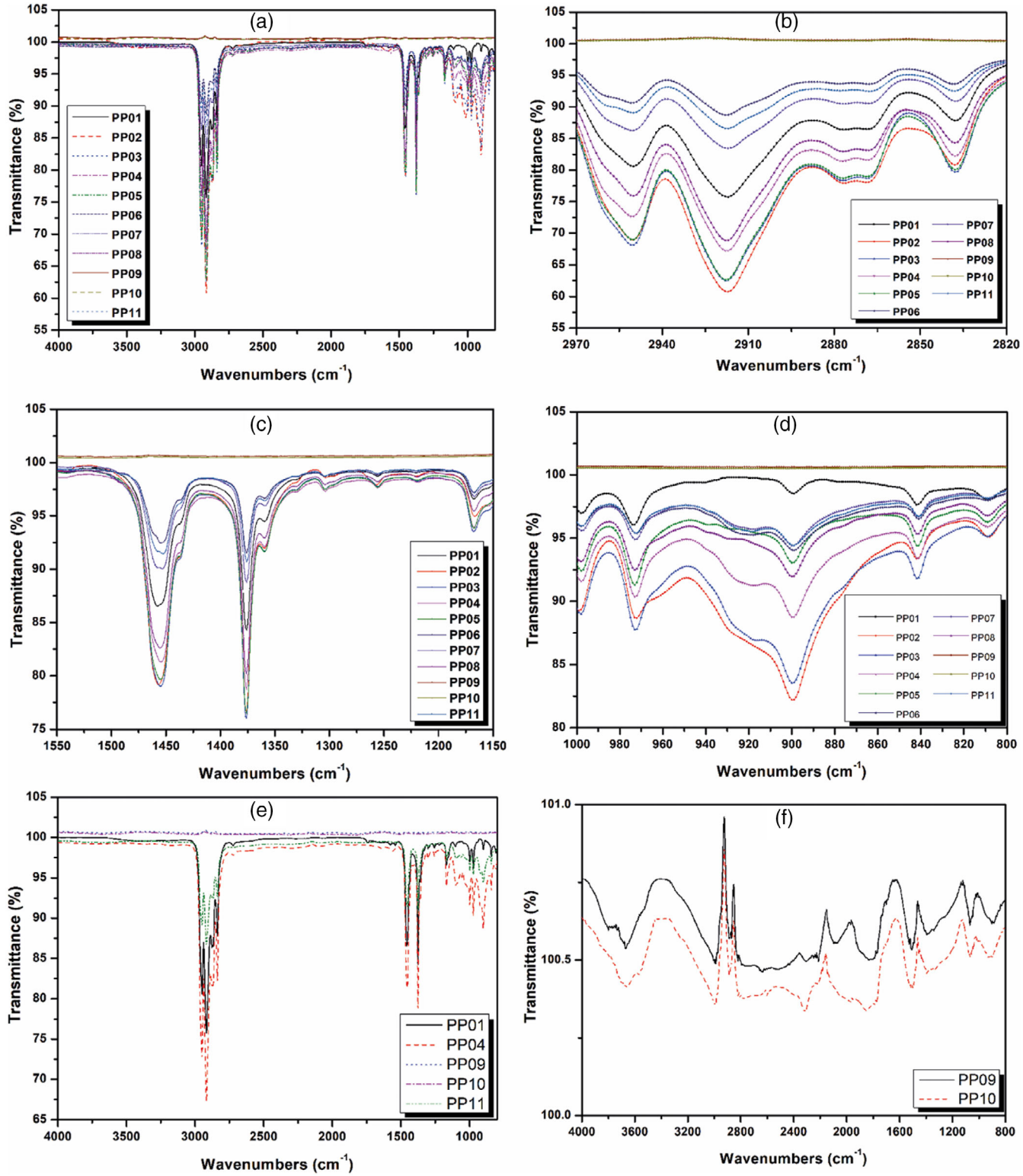

FIGURE 2 Fourier-transform infrared spectroscopy spectra of polypropylene composites. [Color figure can be viewed at wileyonlinelibrary.com]

improvement is due to the superior energy dissipation capacity of SEBS, as known from the literature, in comparison to other materials in the mixture, with the aim of enhancing impact resistance.[38,39] The impact strength of SEBS-g-MA was more prominent compared to SEBS, and this is thought to be attributed to the presence of MA in SEBS-g-MA, which improves interfacial properties, resulting in a longer-chain and more regular structure,

TABLE 3 Tensile and flexural tests results.

Sample code	Tensile strength (MPa)	Tensile modulus (MPa)	Flexural strength (MPa)	Flexural modulus (MPa)
PP01	30.82 (±0.25)	1233 (±59)	33.97 (±0.76)	1359 (±80)
PP02	31.75 (±0.52)	1270 (±23)	48.09 (±1.02)	2405 (±22)
PP03	30.73 (±0.21)	1229 (±26)	46.06 (±0.26)	2422 (±147)
PP04	29.31 (±0.21)	1172 (±28)	45.08 (±0.49)	2234 (±37)
PP05	28.03 (±0.14)	1121 (±66)	44.02 (±1.07)	2068 (±42)
PP06	27.89 (±0.39)	1157 (±87)	42.00 (±1.43)	2090 (±37)
PP07	27.12 (±0.37)	1085 (±07)	42.47 (±1.21)	1848 (±17)
PP08	25.77 (±0.09)	1031 (±84)	40.58 (±0.28)	1677 (±91)
PP09	28.99 (±0.21)	1160 (±07)	44.39 (±0.67)	1690 (±96)
PP10	29.11 (±0.34)	1164 (±74)	41.96 (±0.27)	1416 (±76)
PP11	28.41 (±0.45)	1136 (±17)	40.02 (±1.04)	1399 (±69)

TABLE 4 Hardness and Izod impact tests results.

		Izod impact strength (kJ/m^2)		
		Notch	Notch	Notch
Sample code	Hardness (Sh *D*)	*R*0.25	*R*1	*R*2
PP01	74.0 (±0.03)	2.43 (±0.23)	2.80 (±0.17)	3.10 (±0.34)
PP02	67.0 (±0.05)	2.65 (±0.18)	4.01 (±0.26)	4.21 (±0.56)
PP03	66.0 (±0.34)	2.51 (±0.05)	3.82 (±0.14)	4.05 (±0.08)
PP04	67.0 (±0.22)	2.33 (±0.04)	3.69 (±0.22)	3.88 (±0.11)
PP05	68.0 (±0.14)	2.11 (±0.11)	3.29 (±0.19)	3.68 (±0.27)
PP06	66.0 (±0.11)	2.70 (±0.81)	3.80 (±0.52)	4.08 (±0.56)
PP07	66.0 (±0.21)	3.16 (±0.98)	3.88 (±0.27)	4.47 (±0.85)
PP08	66.0 (±0.33)	4.05 (±0.56)	4.25 (±0.63)	4.90 (±0.09)
PP09	67.0 (±0.16)	2.98 (±0.09)	3.96 (±0.14)	4.10 (±0.10)
PP10	66.5 (±0.23)	3.51 (±0.18)	4.40 (±0.26)	4.73 (±0.36)
PP11	66.0 (±0.35)	4.38 (±0.21)	4.43 (±0.25)	5.26 (±0.14)

and consequently, an improvement in mechanical properties.[40]

The highest hardness value was measured in pure PP. Specifically, the highest hardness value was observed in pure PP. Generally, the hardness values of composites filled with hazelnut shell and wollastonite are closely aligned. While the increase in the proportion of hazelnut shell resulted in a slight hardness increase, this effect is not highly significant. A similar trend is observed between SEBS and SEBS-g-MA. While the hardness of the SEBS composite remains unaffected, the presence of SEBS-g-MA in the structure has altered the hardness, though to a minor extent. It is speculated that as the ratio of SEBS-g-MA increases, the morphology is more affected, the structure becomes more flexible, contributing to a decrease in hardness.[41] The effect of notch size on the formation and progression of cracks is quite evident. As the notch radius increases, the impact resistance increases accordingly. Decreasing notch sizes causes stress intensifications in the composite structure altering the fracture behavior of the composite.

3.3 | DSC test results

DSC test results' numerical values are presented in Table 5, while a graphical comparison of melting and crystallization behaviors is provided in Figure 3. Significant differences are observed in enthalpy changes (ΔH_m), melting temperatures (T_m), and melting peak widths among PP composites. The width of the obtained melting peaks (Figure 4) is believed to originate from the mixture of PP's α- and β-crystal phases and proportional variations in the filler materials.[42] Similarly, the melting

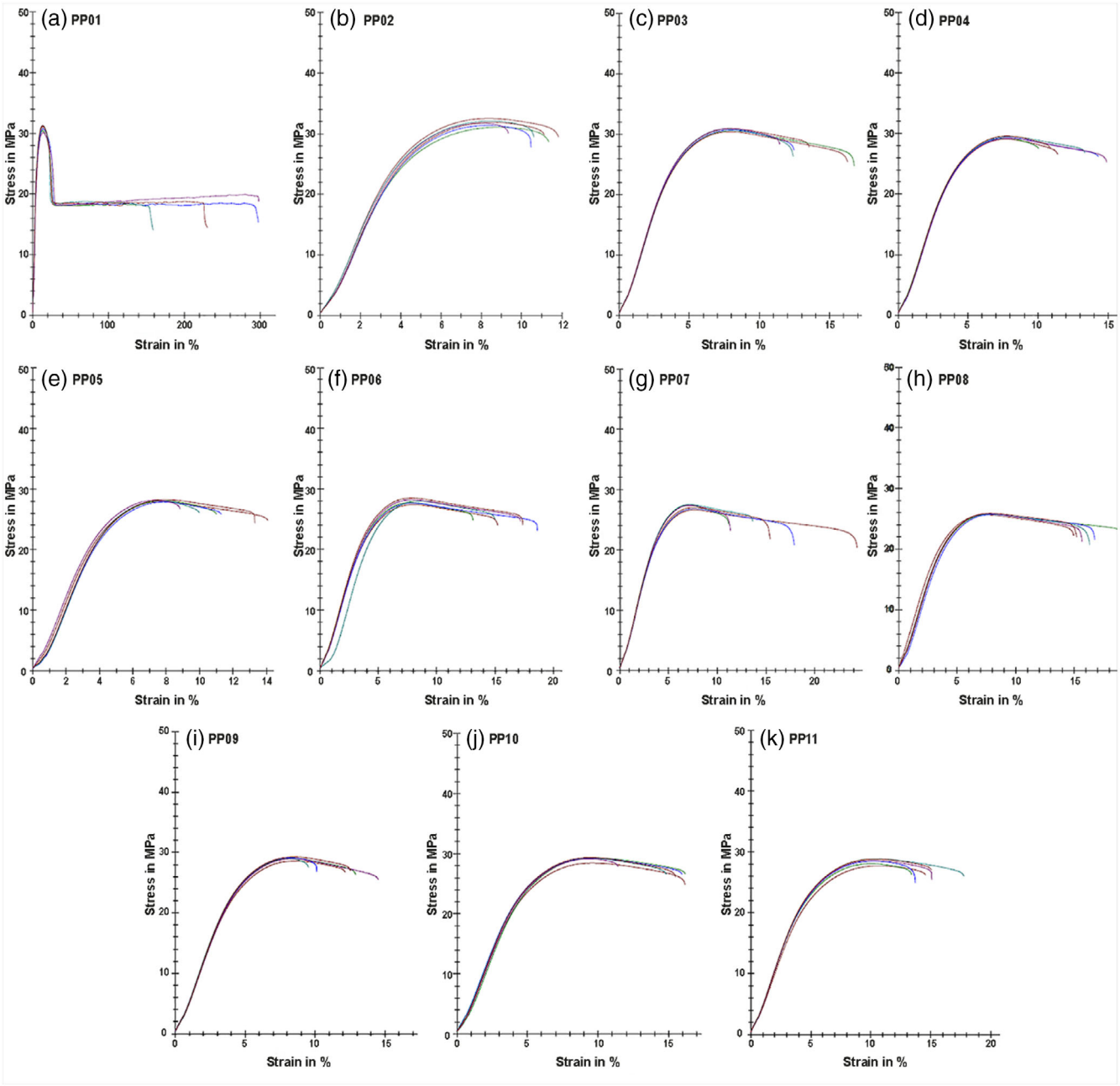

FIGURE 3 Tensile test stress–strain curves. [Color figure can be viewed at wileyonlinelibrary.com]

enthalpies and peak maxima are observed to be influenced by the presence of the filler material. While pure PP (PP01) exhibits the highest ΔH_m value, the PP02 sample with 20% Wollastonite filler stands out with a lower ΔH_m and a T_m close to pure PP. Despite PP02 having lower crystallinity compared to pure PP, its higher lamellar thickness can be explained by wollastonite particles supporting the β-crystallization of the PP matrix.[42–44]

The changes in crystallization rates and crystal lamellae thickness are shown in Figure 5. From Figure 5, it is evident that pure PP exhibits significantly higher crystallinity compared to the PP composites. This observation leads to the hypothesis that the size of the filler material, its distribution orientation within the structure, and the disruption of the polymer chain order contribute to the reduction in crystallinity.[30] When examining crystal lamellar thickness, difference is observed among the samples. This suggests that the samples generally display similar spectral characteristics, indicating a consistent response to proportional changes in filler materials.

3.4 | MFI and HDT test results

The values for melt flow index (MFI) and HDT are provided in Table 5 and Figure 6. Generally, an increase in

the ratio of hazelnut shells in the mixture has been observed to increase both the MFI value and HDT temperature. Although hazelnut shells are speculated to reduce the MFI value through exhibiting a flow-reducing effect due to their cellulose content.[45] Experimental errors in MFI and HDT temperatures can be correlated with the distribution and particle size of hazelnut shells within the matrix.[12,46] On the other hand, SEBS and SEBS-g-MA (styrene-ethylene/butylene-styrene copolymer grafted with Maleic Anhydride) have shown a reducing effect on both MFI value and HDT temperature. With an increase in the ratios of SEBS and SEBS-g-MA in the mixture, MFI values have decreased further. The impact of SEBS-g-MA on the MFI value appears to be more significant than SEBS. This could be attributed to the maleic anhydride groups in SEBS-g-MA increasing the reactive properties of the polymer, as higher reactivity in the structure can alter the processability and flow characteristics, thereby decreasing the MFI value.[46] Regarding HDT temperatures, SEBS-g-MA has demonstrated a more favorable effect compared to SEBS. The increase in the ratios of SEBS and SEBS-g-MA in the PP composites resulted in a decrease in HDT temperatures.

3.5 | TGA test results

To explore the influence of fillers on the thermal stability of PP composites, thermogravimetric analyses were performed on pure PP, as well as on composites filled with

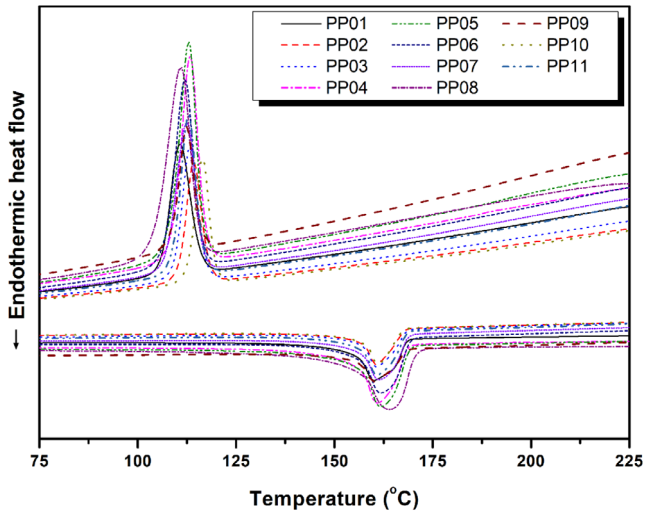

FIGURE 4 Differential scanning calorimetry curves. [Color figure can be viewed at wileyonlinelibrary.com]

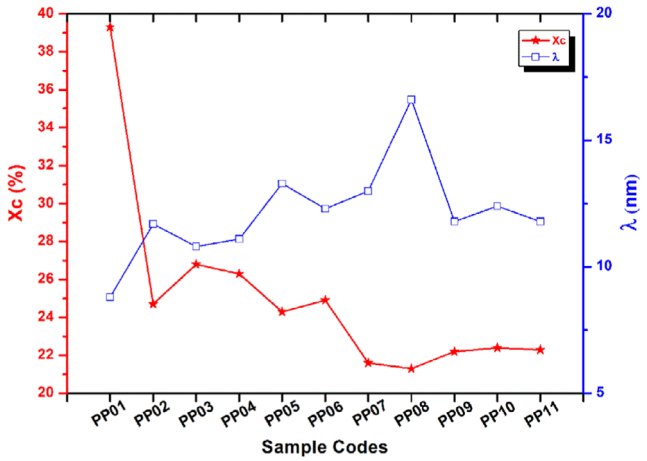

FIGURE 5 Crystallization ratio and changes in crystal lamellae thickness. [Color figure can be viewed at wileyonlinelibrary.com]

TABLE 5 Thermal test results of the samples.

Sample code	MFI (g/10 min)	HDT (°C)	ΔH_m (J/g)	ΔH^o_m (J/g)	δ_e (mJ/m^2)	T_m (°C)	T°_m (°C)	X_c (%)	λ (nm)
PP01	5.13	91.0	82.2	209	29	160.0	174	39.3	8.8
PP02	4.84	69.3	64.4	209	29	160.6	174	24.7	11.7
PP03	4.95	67.6	70.1	209	29	160.7	174	26.8	10.8
PP04	5.10	65.7	68.6	209	29	160.8	174	26.3	11.1
PP05	5.29	68.0	63.4	209	29	162.0	174	24.3	13.3
PP06	4.98	65.2	67.7	209	29	159.8	174	24.9	12.3
PP07	4.35	62.8	61.1	209	29	160.9	174	21.6	13.0
PP08	4.18	63.0	62.7	209	29	161.1	174	21.3	16.6
PP09	4.71	67.3	60.2	209	29	161.3	174	22.2	11.8
PP10	4.20	65.0	63.2	209	29	161.9	174	22.4	12.4
PP11	3.81	64.6	65.5	209	29	164.3	174	22.3	11.8

wollastonite and hazelnut shells, in addition to blends containing SEBS and SEBS-g-MA compatibilizers. The decomposition temperature and the onset of thermal stability, indicated by the temperature at 5% weight loss (% T5), were determined and summarized in Table 6. Figure 7a,b illustrate the TG and DTG curves for both pure PP and PP composites.

A single-step degradation process was observed for both pure PP (PP01) and the 20% wollastonite-filled PP composite (PP02).[47] The degradation of PP (T5) is believed to initiate at 425.6°C with the formation of free radicals, leading to chain scissions. PP composites containing hazelnut shell filler exhibited a two-step decomposition. The first step was associated with the degradation of hazelnut filler and occurred depending on the composition and content of the mixture. The second step corresponded to the decomposition of polymer part of the composites. Due to the thermal stabilizing effect of wollastonite,[48] PP composites demonstrated enhanced thermal stability compared to pure PP. The contributions of SEBS and SEBS-g-MA influenced the thermal degradation of the composites, as evidenced by the shift in the decomposition initiation temperature (%T5) and the mass loss curve toward lower temperatures in a nitrogen atmosphere. Figure 5b's DTG curve supports this observed thermal stability. The thermal stability of polymer blends predominantly relies on the morphology and miscibility of the system. The results of thermal degradation suggest that the addition of the filler can enhance the thermal stability of pure PP. However, the thermal stability of the composites decreased with the addition of SEBS and SEBS-g-MA. This effect was more pronounced due to the increased reactive properties of the polymer with maleic anhydride groups in SEBS-g-MA.[44]

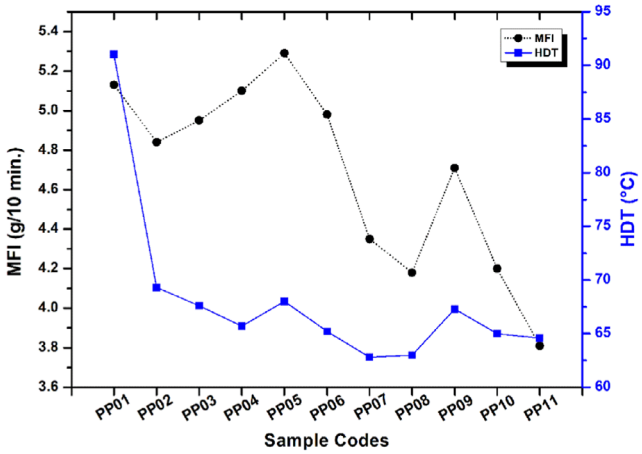

FIGURE 6 Comparison of heat deflection temperature and melt flow index values for samples. [Color figure can be viewed at wileyonlinelibrary.com]

3.6 | Results of morphological investigations

The SEM microstructures obtained from the fractured surfaces of samples are presented in Figure 8. The microstructure of pure PP labeled as PP01 (Figure 8a) demonstrates the typical fracture characteristic of PP.[49] It is observed that wollastonite is homogeneously distributed within the structure and further increases the brittleness of the structure, leading to fibrillation (Figure 8b). Although partial, void formations due to separations between wollastonite particles and the matrix interface are observed within the structure. It can be expected that these voids reduce mechanical properties such as tensile strength and flexural strength. However, similar studies have reported partial increases in mechanical properties with wollastonite loading up to 20%, indicating that this phenomenon is related to the filler content.[50] Essentially, this can be explained by

TABLE 6 The numerical data obtained from the thermogravimetric analysis tests.

Sample code	T_5 (°C)	T_{50} (°C)	T_{max} (°C)	Residue at 600°C (%)
PP01	425.6	458.2	480.3	2.4
PP02	437.6	464.1	482.1	23.0
PP03	435.0	465.0	489.6	17.5
PP04	438.5	466.1	488.1	13.9
PP05	435.9	464.4	487.6	8.4
PP06	432.8	463.9	485.8	13.5
PP07	431.3	461.5	484.9	12.7
PP08	431.9	462.4	483.2	9.3
PP09	426.7	462.5	485.4	13.8
PP10	431.9	462.3	487.2	13.3
PP11	425.0	459.6	484.2	12.3

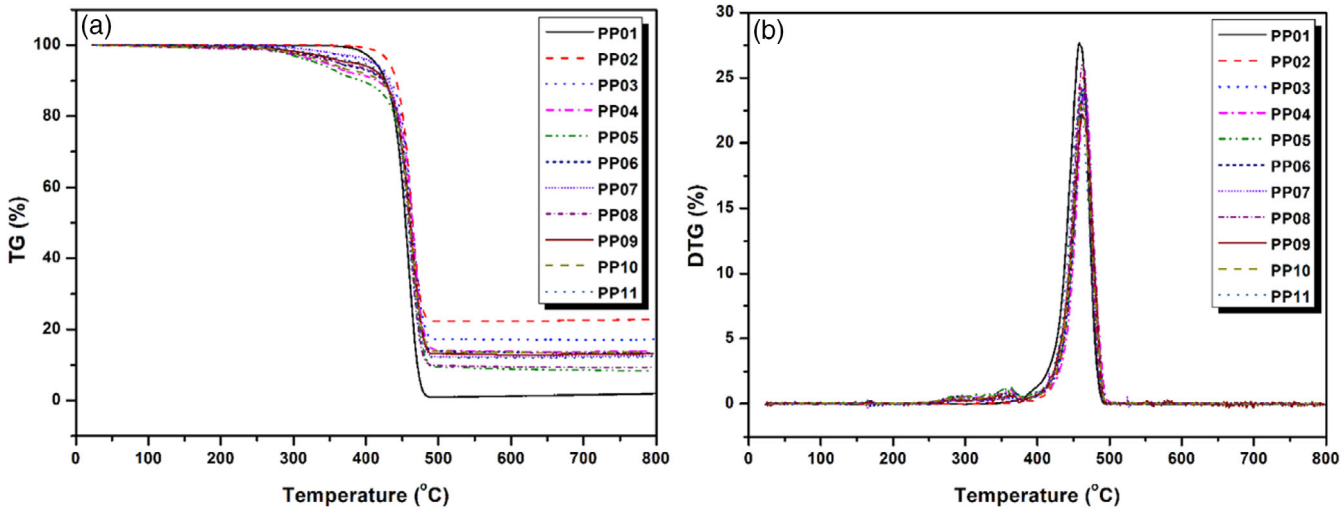

FIGURE 7 Thermogravimetric analysis curves of samples. [Color figure can be viewed at wileyonlinelibrary.com]

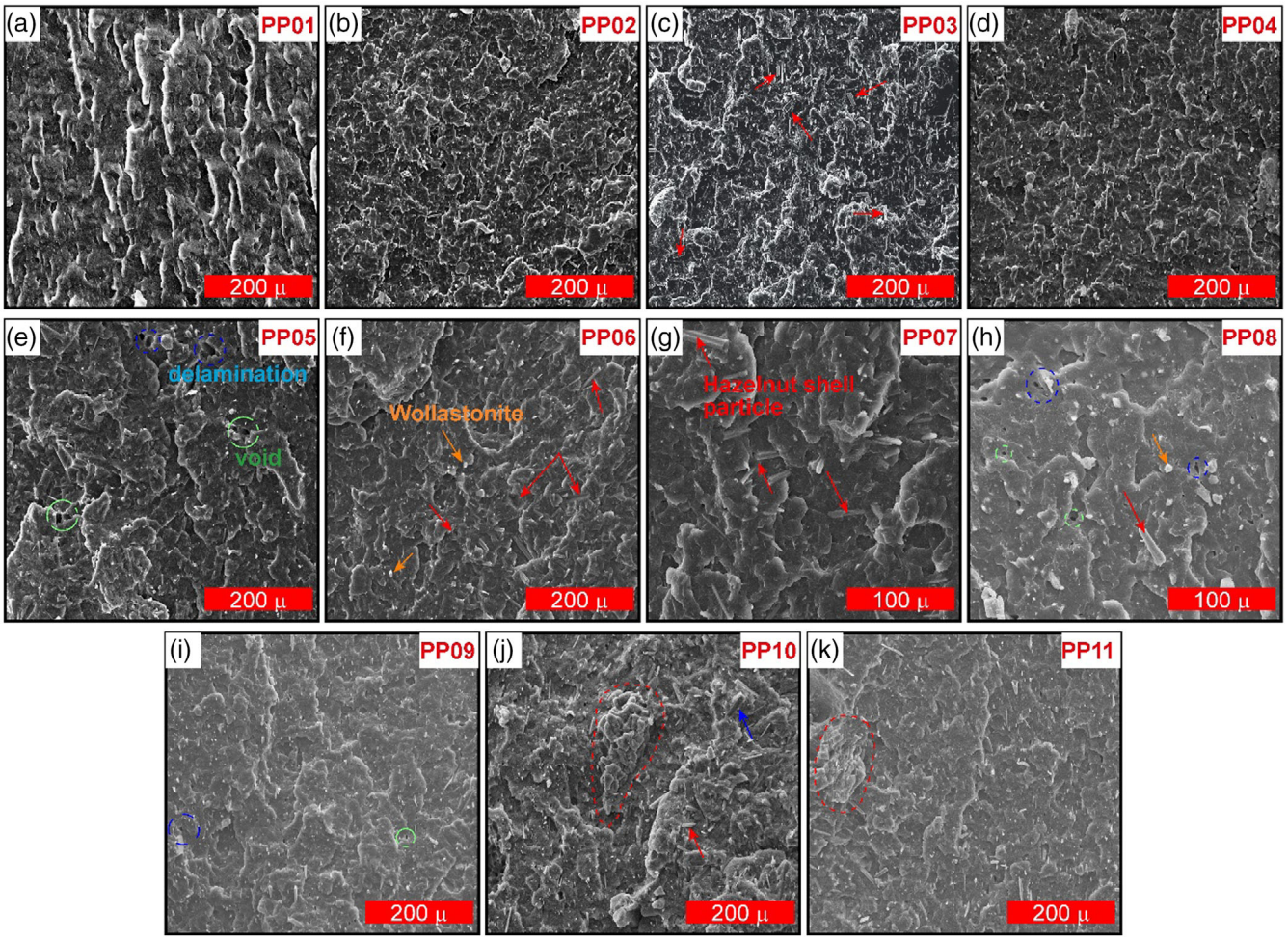

FIGURE 8 The scanning electron microscopy microstructure images of pure polypropylene (PP) and PP composites. [Color figure can be viewed at wileyonlinelibrary.com]

the limited void formation within the structure and the ability of wollastonite to bear a greater load than the matrix.[51]

The decrease in wollastonite filler content and the increase in hazelnut shell addition have reduced fibrillation in the microstructure (Figure 8c–e). The addition of

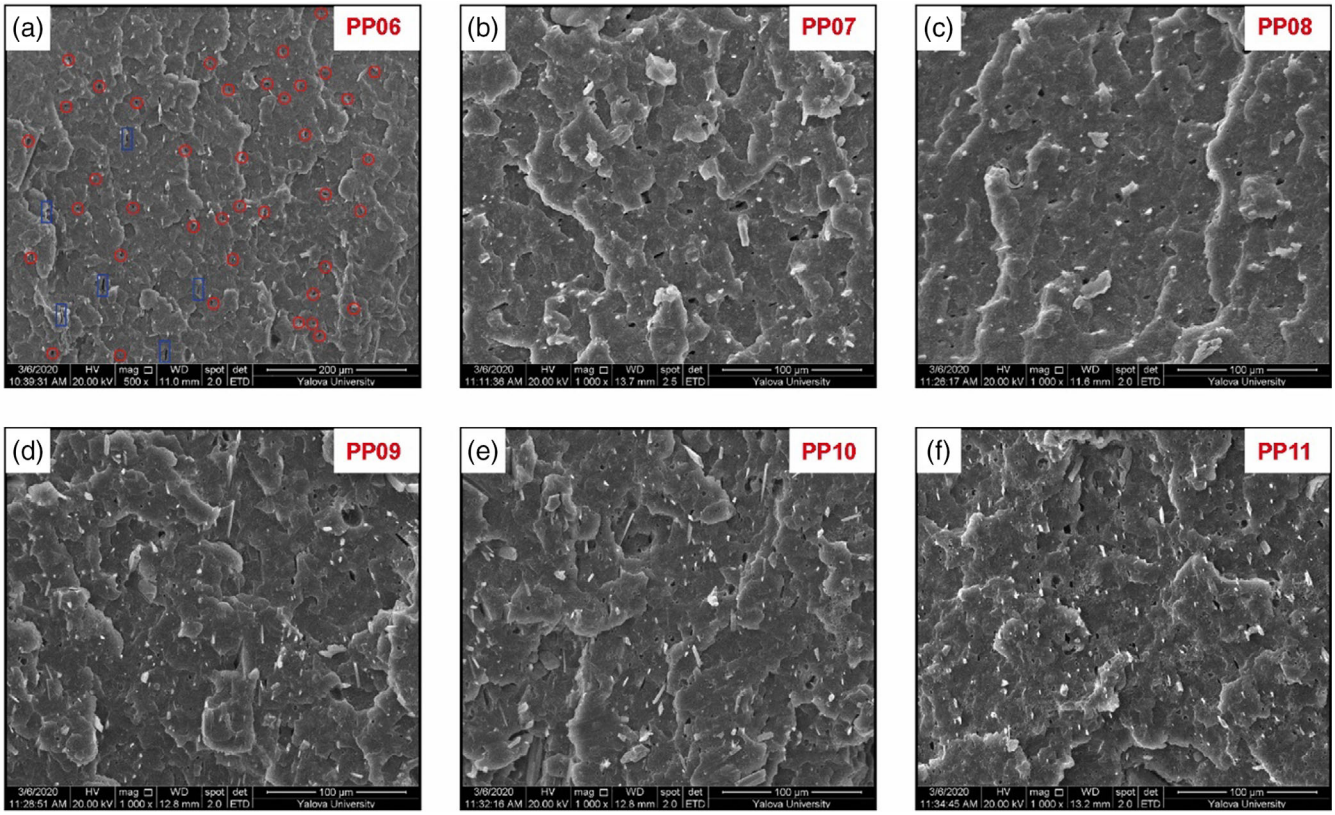

FIGURE 9 The scanning electron microscopy microstructure images of samples. [Color figure can be viewed at wileyonlinelibrary.com]

SEBS and SEBS-g-MA has forced the structure to become more regular. The changes in the microstructure confirm this (Figure 8f–k). With an increase in the SEBS-g-MA ratio, agglomeration is observed within the structure (Figure 8j,k). This agglomeration could be attributed to the increase in the MA content in SEBS-g-MA or to an uneven distribution. The high concentration in the regions of agglomeration may originate from the irregular surface of lignocellulosic material, namely hazelnut shell.

In Figure 9, it can be observed that the SEBS and SEBS-g-MA compatibilizer particles, perceived as black holes, exhibit shapes resembling spherical or near-spherical or irregular anisotropic lamellae of different sizes. The spherical shapes in the structure are believed to result from rounding due to interfacial tension between the PP matrix and the elastomeric phase.[52] In composites where the SEBS and SEBS-g-MA ratio is 3%, the size of these spherical elastomeric phases is relatively smaller compared to the composites with 6% and 9% filler content (Figure 9a). As the ratio increases, it is observed that the size of the spherical shape increases, and their number is relatively fewer compared to the 3% filler content. Overall, it can be stated that SEBS and SEBS-g-MA are homogeneously distributed within the structure, and this distribution affects the microstructure according to the sizes of the resulting spherical elastomeric phases, thereby influencing mechanical and thermal properties.

4 | CONCLUSIONS

This study investigated the mechanical and thermal properties of PP composites by utilizing PP as the matrix and incorporating wollastonite, hazelnut shell fillers, and SEBS/SEBS-g-MA as modifiers. The SEM microstructures were examined, and the results were compared. Based on the findings of this comprehensive study, several important conclusions emerge. First, regarding the influence of fillers on mechanical properties, we observed that wollastonite had a more pronounced effect due to its long and slender fibrous structure. Additionally, the addition of SEBS and SEBS-g-MA led to a decrease in tensile strength, tensile modulus, flexural strength, and flexural modulus, while simultaneously increasing impact strength. This increase in impact strength indicates the effectiveness of SEBS and SEBS-g-MA in enhancing impact resistance. Regarding thermal behavior and stability, the presence of fillers and compatibilizers affected the crystallization rates, thickness of crystal lamellae, and thermal stability of the composites. Wollastonite contributed to thermal stability, while SEBS-g-MA showed a

more positive effect compared with SEBS. SEM microstructure images revealed the distribution of SEBS and SEBS-g-MA in the composite structure. The observed spherical elastomeric phases in the microstructure were influenced by filler content and the ratio of SEBS to SEBS-g-MA. Higher ratios of SEBS and SEBS-g-MA resulted in larger spherical shapes as well as a reduced number of particles. In conclusion, this study emphasizes the importance of filler selection, addition of compatibilizers, and their distribution in the composite structure for achieving desired mechanical and thermal properties. These findings contribute to the development of cost-effective and sustainable materials for industrial applications. Future research in this field should focus on optimizing formulations for specific applications and investigating the long-term performance of these composites under real-world conditions.

AUTHOR CONTRIBUTIONS

İdris Karagöz: Conceptualization (lead); methodology (equal); writing – review and editing (lead). **Kenan Büyükkaya:** Conceptualization (equal); data curation (equal); methodology (equal). **Halil Demirer:** Conceptualization (equal); methodology (equal); writing – review and editing (equal). **Mehmet Mudu:** Conceptualization (equal); methodology (equal). **İlyas Kartal:** Conceptualization (equal); methodology (equal).

DATA AVAILABILITY STATEMENT

The raw data required to reproduce these findings can be obtained from the authors via email.

ORCID

İdris Karagöz https://orcid.org/0000-0002-2644-8511

REFERENCES

[1] V. Ambrogi, P. Cerruti, C. Carfagna, M. Malinconico, V. Marturano, M. Perrotti, P. Persico, *Polym. Degrad. Stab.* **2011**, *96*, 2152.
[2] A. Ashori, *Bioresour. Technol.* **2008**, *99*, 4661.
[3] H. A. Khalil, A. H. Bhat, A. I. Yusra, *Carbohydr. Polym.* **2012**, *87*, 963.
[4] E. Abraham, P. A. Elbi, B. Deepa, P. Jyotishkumar, L. A. Pothen, S. S. Narine, S. Thomas, *Polym. Degrad. Stab.* **2012**, *97*, 2378.
[5] G. Koronis, A. Silva, M. Fontul, *Compos Part B: Eng* **2013**, *44*, 120.
[6] D. V. Suriapparao, D. K. Ojha, T. Ray, R. Vinu, *J. Therm. Anal. Calorim.* **2014**, *117*, 1441.
[7] A. J. Nunez, P. C. Sturm, J. M. Kenny, M. I. Aranguren, N. E. Marcovich, M. M. Reboredo, *J. Appl. Polym. Sci.* **2003**, *88*, 1420.
[8] N. Çakir Yiğit, İ. Karagöz, *Polym.-Plast. Technol. Mater.* **2023**, *62*, 1077.
[9] I. O. Oladele, I. O. Ibrahim, A. D. Akinwekomi, S. I. Talabi, *Polym. Test.* **2019**, *76*, 192.
[10] İ. H. Basboga, İ. Atar, K. Karakus, F. Mengeloglu, *Pro Ligno* **2017**, *13*, 276.
[11] M. Tufan, N. Ayrılmış, *BioRes.* **2016**, *11*, 7476.
[12] H. Demirer, İ. Kartal, A. Yıldırım, K. Büyükkaya, *Acta Phys. Pol. A* **2018**, *134*, 254.
[13] İ. Karagöz, *Polym. Bullet.* **2024.** (Articles in Press) https://doi.org/10.1007/s00289-024-05247-4
[14] J. F. Balart, V. Fombuena, O. Fenollar, T. Boronat, L. Sánchez-Nacher, *Compos Part B: Eng* **2016**, *86*, 168.
[15] K. Salasinska, J. Ryszkowska, *Compos. Interfaces* **2012**, *19*, 321.
[16] M. Barczewski, K. Sałasińska, J. Szulc, *Polym. Test.* **2019**, *75*, 1.
[17] H. Essabir, S. Nekhlaoui, M. Malha, M. O. Bensalah, F. Z. Arrakhiz, A. Qaiss, R. Bouhfid, *Mater. Des.* **2013**, *51*, 225.
[18] D. Battegazzore, S. Bocchini, J. Alongi, A. Frache, *Polym. Degrad. Stab.* **2014**, *108*, 297.
[19] A. L. Catto, B. V. Stefani, V. F. Ribeiro, R. M. C. Santana, *Mater. Res.* **2014**, *17*, 203.
[20] A. K. Sadhukhan, P. Gupta, T. Goyal, R. K. Saha, *Bioresour. Technol.* **2008**, *99*, 8022.
[21] A. Kufel, S. Kuciel, *Polymer* **2019**, *12*, 18.
[22] F. P. La Mantia, M. Morreale, *Compos Part A: Appl Sci Manuf* **2011**, *42*, 579.
[23] V. K. Thakur, A. S. Singha, M. K. Thakur, *Int. J. Polym. Anal. Charact.* **2012**, *17*, 401.
[24] Z. Liu, S. Z. Erhan, D. E. Akin, F. E. Barton, *J. Agric. Food Chem.* **2006**, *54*, 2134.
[25] M. A. Fuad, M. J. Zaini, M. Jamaludin, Z. M. Ishak, A. M. Omar, *J. Appl. Polym. Sci.* **1994**, *51*, 1875.
[26] H. Jeske, A. Schirp, F. Cornelius, *Thermochim. Acta* **2012**, *543*, 165.
[27] J. P. Pires, A. D. S. Ramos, G. M. Miranda, G. L. de Souza, F. Fraga, C. M. N. Azevedo, R. A. Ligabue, J. E. E. de Lima, R. V. Lourega, *Polym. Bull.* **2021**, *78*, 2025.
[28] K. Büyükkaya, *Artvin Çoruh Üniversitesi Orman Fakültesi Dergisi* **2022**, *23*, 160.
[29] Nyco Minerals Ltd, Nyco NYGLOS® 8 Wollastonite Technical Data Sheet. https://www.lookpolymers.com/pdf/Nyco-NYGLOS-8-Wollastonite.pdf (accessed: May 3, 2024)
[30] M. Kandemir, İ. Karagöz, H. Sepetçioğlu, *El-Cezeri* **2023**, *10*, 109.
[31] J. Fang, L. Zhang, D. Sutton, X. Wang, T. Lin, *J. Nanomater.* **2012**, *2012*, 1.
[32] T. A. Huy, R. Adhikari, T. Lüpke, S. Henning, G. H. Michler, *J. Polym. Sci., Part B: Polym. Phys.* **2004**, *42*, 4478.
[33] D. Perrin, R. Léger, B. Otazaghine, P. Ienny, *J. Mater. Sci.* **2017**, *52*, 7591.
[34] K. Leontiadis, D. S. Achilias, I. Tsivintzelis, *Polymer* **2023**, *15*, 2986.
[35] S. Senthilkumar, V. L. Raja, P. Gaur, P. P. Patil, L. Natrayan, S. Kaliappan, *J. Appl. Mech. Mater.* **2023**, *912*, 113.
[36] L. Ranakoti, P. Bhandari, M. K. Gupta, K. Kumar, S. Bhatia, S. Kosaraju, J. Singh, *Mater. Today Proc.* **2023**. (Articles in Press)
[37] N. I. Cherkashina, Z. V. Pavlenko, D. Y. V. Y. Pushkarskaya, L. V. Denisova, S. N. Domarev, D. Y. A. Ryzhikh, *Polymer* **2023**, *15*, 3212.
[38] K. Alavi, S. Tarashi, H. Nazockdast, M. Rafizadeh, *Polym. Compos* **2023**, *44*, 8125.

[39] B. K. Dinesh, J. Kim, *Polymer* **2023**, *15*, 1225.
[40] Z. Benneghmouche, D. Benachour, M. Fatmi, M. A. Habila, M. Sillanpaa, *J. Polym. Res.* **2024**, *31*, 5.
[41] S. Liu, J. Qiu, L. Han, J. Luan, X. Ma, W. Chen, *Polymer* **2023**, *15*, 2753.
[42] A. S. Luyt, M. D. Dramićanin, Ž. Antić, V. Djoković, *Polym. Test.* **2009**, *28*, 348.
[43] L. Jingjiang, W. Xiufen, *J. Appl. Polym. Sci.* **1990**, *41*, 2829.
[44] M. R. Meng, Q. Dou, *Mater. Sci. Eng., A* **2008**, *492*, 177.
[45] E. Kuram, *J. Mater. Cycles Waste Manage.* **2020**, *22*, 2107.
[46] E. Kuram, *Emerg Mater.* **2022**, *5*, 811.
[47] V. O. Bulatović, A. Mihaljević, E. G. Bajsić, T. G. Holjevac, *Int. Polym. Process.* **2017**, *32*, 102.
[48] S. Chuayjuljit, S. Ketthongmongkol, *J. Thermoplast. Compos. Mater.* **2013**, *26*, 923.
[49] W. Wang, X. Zhang, Z. Mao, W. Zhao, *Results Phys.* **2019**, *12*, 2169.
[50] D. Zhang, M. He, S. Qin, J. Yu, *J. RSC Adv.* **2017**, *7*, 15439.
[51] J. X. Chan, J. F. Wong, A. Hassan, Z. Mohamad, N. Othman, *Polym. Compos.* **2020**, *41*, 395.
[52] E. Tekay, N. Nugay, T. Nugay, S. Şen, *Polym. Compos.* **2019**, *40*, 24.

How to cite this article: İ. Karagöz, K. Büyükkaya, H. Demirer, M. Mudu, İ. Kartal, *J. Appl. Polym. Sci.* **2024**, e55710. https://doi.org/10.1002/app.55710